

University of Windsor

Scholarship at UWindsor

Chemistry and Biochemistry Publications

Department of Chemistry and Biochemistry

Summer 8-25-2016


Insights from molecular dynamics on substrate binding and effects of active site mutations in Delta1-pyrroline-5-carboxylate dehydrogenase

Bogdan F. Ion
University of Windsor

Mohamed M. Aboelnga
University of Windsor

James W. Gauld
University of Windsor

Follow this and additional works at: <https://scholar.uwindsor.ca/chemistrybiochemistrypub>

 Part of the [Biophysics Commons](#), and the [Physical Chemistry Commons](#)

Recommended Citation

Ion, Bogdan F.; Aboelnga, Mohamed M.; and Gauld, James W.. (2016). Insights from molecular dynamics on substrate binding and effects of active site mutations in Delta1-pyrroline-5-carboxylate dehydrogenase. *Canadian Journal of Chemistry*, 94, 1151-1162.
<https://scholar.uwindsor.ca/chemistrybiochemistrypub/87>

This Article is brought to you for free and open access by the Department of Chemistry and Biochemistry at Scholarship at UWindsor. It has been accepted for inclusion in Chemistry and Biochemistry Publications by an authorized administrator of Scholarship at UWindsor. For more information, please contact scholarship@uwindsor.ca.

Insights from molecular dynamics on substrate binding and effects of active site mutations in Δ^1 -pyrroline-5-carboxylate dehydrogenase

Bogdan F. Ion, Mohamed M. Aboelnga, and James W. Gauld

Abstract: The NAD⁺-dependent enzyme, Δ^1 -pyrroline-5-carboxylate dehydrogenase (P5CDH), has an important role in proline and hydroxyproline catabolism for humans. Specifically, this aldehyde dehydrogenase is responsible for the oxidation of both L-glutamate- γ -semialdehyde (GSA) and 4-erythro-hydroxy-L-glutamate- γ -semialdehyde (4-OH-GSA) to their respective L-glutamate product forms. We have performed a detailed molecular dynamics (MD) study of both the reactant and product complex structures of P5CDH to gain insights into ligand binding (i.e., GSA, 4-OH-GSA, NAD⁺, GLU) in the active site. Moreover, our investigations were further extended to examine the structural impact of S352L, S352A, and E314A mutations on the deficiency in the P5CDH enzymatic activity. Our *in silico* mutation analysis indicated that the conserved Glu447 has significantly shifted in both the S352L and E314A mutants, causing NAD⁺ to be displaced from its predictive orientation in the binding site and hence forming a catalytically inactive enzyme. However in the case of S352A, the catalytic site including the oxyanion hole and Cys348 remain virtually unchanged, and the coenzyme maintains its binding position.

Key words: aldehyde dehydrogenase, NAD, mutagenesis, molecular dynamics, binding conformation.

Résumé : La Δ^1 -pyrroline-5-carboxylate déshydrogénase (P5CDH), une enzyme dépendante du NAD⁺, joue un rôle important dans le catabolisme de la proline et de l'hydroxyproline chez l'humain. En particulier, cette aldéhyde déshydrogénase est responsable de l'oxydation du L-glutamate- γ -semialdéhyde (GSA) et du 4-érythro-hydroxy-L-glutamate- γ -semialdéhyde (4-OH-GSA) en leurs formes respectives du L-glutamate. Nous avons réalisé une étude détaillée de dynamique moléculaire (DM) portant sur les structures des réactifs (c.-à-d. le GSA, le 4-OH-GSA, le NAD⁺ et le GLU) et celles de leurs complexes avec la P5CDH en vue de mieux comprendre la liaison du ligand au site actif. De plus, nous avons approfondi nos recherches afin d'examiner l'incidence structurale des mutations S352L, S352A et E314A sur la réduction de l'activité enzymatique de la P5CDH. Notre analyse *in silico* des mutations a montré que le résidu Glu447 conservé dans les mutants S352L et E314A s'est considérablement déplacé, ce qui a entraîné un changement de position du NAD⁺ par rapport à son orientation prévue dans le site de liaison, et par conséquent, la formation d'une enzyme inactive sur le plan catalytique. Toutefois, dans le cas de la mutation S352A, le site catalytique comprenant le trou oxyanion et le résidu Cys348 demeure essentiellement inchangé, et la coenzyme conserve la position de sa liaison. [Traduit par la Rédaction]

Mots-clés : aldéhyde déshydrogénase, NAD, mutagenèse, dynamique moléculaire, conformation de liaison.

Introduction

Pyridine nucleotides are coenzymes that play important roles in protein biochemistry, including metabolic and regulatory signaling pathways.^{1–3} More specific functions of these nucleotides include redox reactions,⁴ ion channel regulation,^{5–6} apoptosis,^{7–8} cell survival,⁹ and cell signaling,^{10–11} with these occurring under both physiological and pathological conditions.

The NAD⁺ dinucleotide and its phosphorylated form, NADP⁺, commonly serve as coenzymes in cellular metabolism.^{1,12–13} In such cases they not only behave as electron carriers in oxidative phosphorylation but also can act as substrates for ADP-ribosylation reactions as well as precursors of the calcium-mobilizing cyclic ADP-ribose.¹⁴ More importantly, they are involved in proline metabolism with functions such as osmolytic control¹⁵ and regulation of cellular stress responses.^{16–17}

NAD⁺/NADP⁺-dependent dehydrogenases are an important group of enzymes that play significant roles in metabolism^{18–20} and as a

result are also thought to be important to several physiological disorders.^{21–22} In particular, type II hyperprolinemia is an autosomal genetic disorder that is believed to cause neurodegeneration in humans.^{23–24} This pathology is linked to a deficiency in Δ^1 -pyrroline-5-carboxylate dehydrogenase (P5CDH) activity; that is, a decrease in the catalyzed conversion of L-glutamate- γ -semialdehyde (GSA) to L-glutamate (Scheme 1).²³ This results in an overproduction of Δ^1 -pyrroline-5-carboxylate (P5C),²⁵ causing an elevation in concentration of cellular plasma L-proline, an important amino acid believed to have a central nervous system-related role in mammals.²⁶ P5CDH is also involved in hydroxyproline catabolism, making it a dual substrate specific enzyme. P5CDH can also bind the hydroxylated form of its GSA substrate, 4-erythro-hydroxy-L-glutamate- γ -semialdehyde (4-OH-GSA) and form the respective hydroxylated L-glutamate product (4-OH-GLU).²⁷

Early site-directed mutagenesis studies by Wang et al.²⁸ suggested that mitochondrial aldehyde dehydrogenase (ALDH) relies

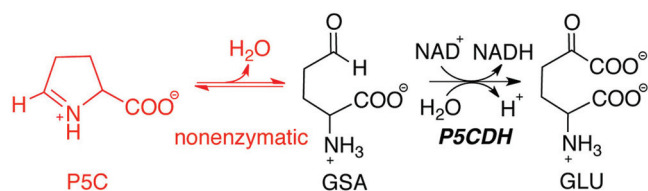
Received 5 June 2016. Accepted 16 August 2016.

B.F. Ion, M.M. Aboelnga, and J.W. Gauld. Department of Chemistry and Biochemistry, University of Windsor, Windsor, ON N9B 3P4, Canada.
Corresponding author: James W. Gauld (email: gauld@uwindsor.ca).

This paper is part of a Special issue dedicated to Professors Russell Boyd and Arvi Rauk.

Copyright remains with the author(s) or their institution(s). Permission for reuse (free in most cases) can be obtained from RightsLink.

Scheme 1. Overall reaction for the conversion of L-glutamate- γ -semialdehyde (GSA) to glutamate by P5CDH.²³ [Colour online.]



on a glutamate residue (Glu268) for initial activation of a catalytically essential cysteinyl, Cys302. Point mutation studies by Farres et al.²⁹ further supported the suggestion that Cys302 residue acts as the mechanistic nucleophile.

Unlike other NAD⁺-binding proteins, aldehyde dehydrogenases have unique structural features that allow them to make fewer contacts with the coenzyme after binding.^{30–32} Crystallographic studies by Hammen et al.³³ showed that the nicotinamide ring of NAD⁺ can have multiple conformations upon binding to ALDH. In particular, one NAD⁺ conformation prevents the proposed general base, Glu268, from activating (deprotonating) the thiol of Cys302. In contrast, in another conformation the nicotinamide moiety is not close enough to the aldehyde substrate for an efficient hydride transfer. Perez-Miller et al.³⁴ used X-ray crystallography and mutagenic studies to determine the structures of the wild-type and C302S mutant complexed with both NAD⁺ and NADH. They concluded that the oxidized cofactor prefers the extended conformation necessary for hydride transfer, whereas NADH binds in a contracted conformation, allowing the deacylation reaction to occur.

Subsequently, Inagaki et al.¹⁸ obtained several X-ray crystallographic structures of a P5CDH from *Thermus thermophilus*, including the apoenzyme, as well as complexes of the enzyme with NAD⁺, NADH, and product (GLU) bound within the active site. They concluded that no activator was in fact available to deprotonate the thiol of Cys302. Rather, an oxyanion hole might increase the electrophilic character of the substrate's aldehyde carbon (C_{carb}), increasing its susceptibility to nucleophilic attack by the sulfur of Cys302. However it should be noted that Tsybovsky et al.³² have suggested that the active site glutamate in aldehyde dehydrogenases may not only be involved in the thioester hydrolysis but also in the activation of the catalytic cysteinyl.

Consequently, the overall catalytic mechanism of P5CDH has been proposed to occur in essentially three stages (Scheme 2); (i) substrate and coenzyme binding, (ii) acylation, and (iii) deacylation.¹⁸

More specifically, in the first stage the NAD⁺ coenzyme and GSA substrate bind within the active site resulting in conformational changes of several active site residues. In particular, the R-group carboxylate of Glu314 (equivalent of Glu268) rotates to point away from the active site. Meanwhile, the peptide backbone between Cys315 and Gly316 shifts, allowing the backbone carbonyl oxygen of Cys315 to hydrogen bond with the nicotinamide's -NH moiety.

In the subsequent acylation (Stage 2) the thiol sulfur of Cys348 (equivalent of Cys302) nucleophilically attacks the substrate aldehyde carbon (C_{carb}) to form a tetrahedral hemithioacetal intermediate. As noted above, whether or not the Cys is activated is unclear; in Scheme 2 we have shown the thiol as neutral. The hemithioacetal's oxyanion is thought to be stabilized by an oxyanion hole comprising hydrogen bonds with the R-group amide of Asn211 and the backbone -NH- of Cys348. Similar to several amidase studies,^{35–37} these two participating residues are known to form the oxyanion hole. Collapse of this tetrahedral intermediate results in the formation of a thioacyl enzyme with concurrent production of NADH. The latter coenzyme then leaves the active site, enabling the R-group of Glu314 and peptide backbone between Cys315 and Gly316 to return to their initial conformations.

This is then followed by deacylation (Stage 3). A water molecule binds within the active site. This water is activated via a hydrogen bond with the R-group carboxylate of Glu314, enabling its oxygen to nucleophilically attack at the covalent enzyme-intermediate's δ C to occur. The tetrahedral intermediate formed is then able to collapse with cleavage of the Cys348- δ C bond, forming the product glutamate (GLU). The Cys348 R-group can then reposition enabling the release of GLU and regeneration of the unbound active site.

Using molecular dynamics (MD) simulations and available X-ray crystal structures,¹⁸ Hempel et al.³⁸ investigated the impact of the hyperprolinemia-associated mutation S352L on the structure of P5CDH. They concluded that this mutation disrupts the water network between a serinyl residue and the catalytic cysteinyl. However Srivastava et al.²³ have performed X-ray crystallographic and mutagenic studies and suggested that the S352L mutation instead disrupts substrate recognition, NAD⁺ binding, and orientation of the Cys348.

In this study, we have used molecular dynamics to investigate the effects of substrate, product, and coenzyme binding within the active site of P5CDH. In particular, we have examined the roles of proposed key active site residues on the binding of substrate, coenzyme, and (or) product. In addition, we have also performed a series of genetically important *in silico* mutations to better understand the roles of the various key residues as well as the impact of such mutations.

Computational methods

All molecular dynamics (MD) calculations were done using the Molecular Operating Environment (MOE)³⁹ and NAMD⁴⁰ programs.

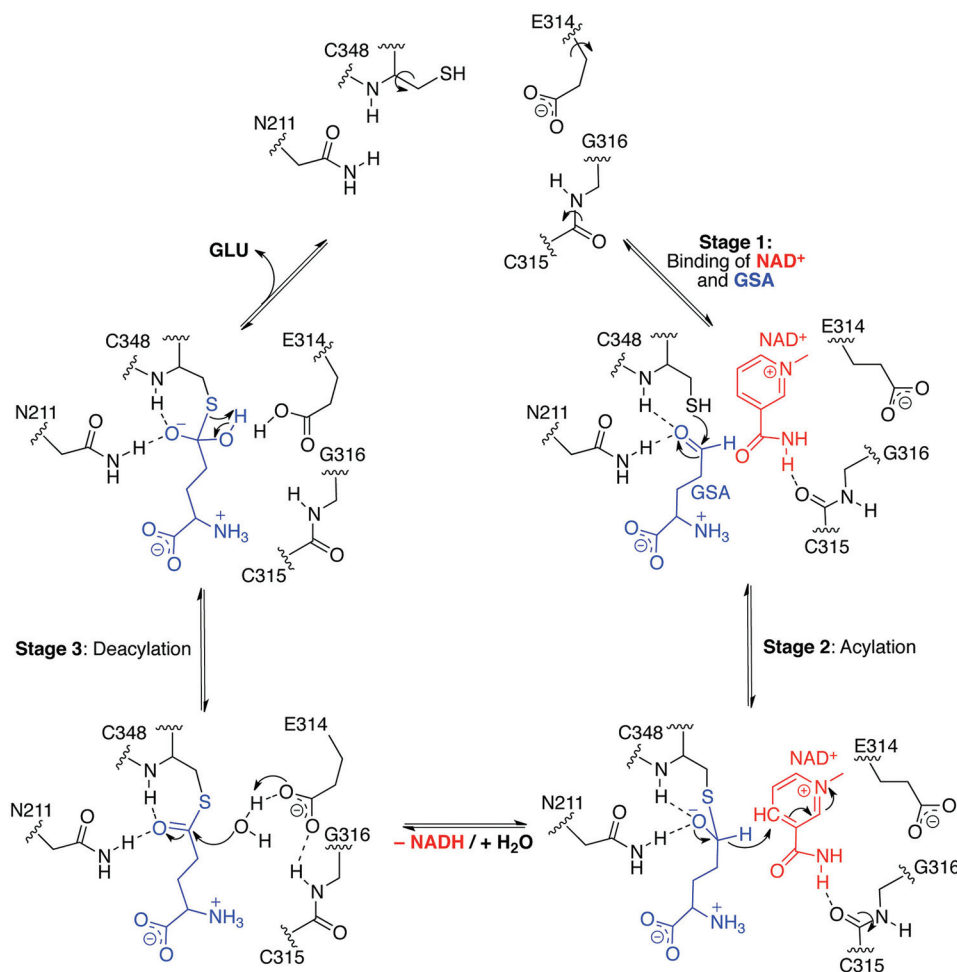
Chemical models

The reactant and product complexes were modeled based on several X-ray crystallographic structures of a homo-dimeric Δ^1 -pyrroline-5-carboxylate dehydrogenase (P5CDH) from a mouse. Specifically, the reactant complex (RC) was prepared from a holoenzyme, bound with the NAD⁺ coenzyme (PDB ID: 3V9L).²³ This structure was then docked with the L-glutamate- γ -semialdehyde (GSA) substrate, where the binding interactions were based on the GLU-bound P5CDH (PDB ID: 3V9K)²³ due to the similarity of the ligands. The template structure for the product complex (PC) is the unbound P5CDH active site (PDB ID: 3V9J),²³ where the glutamate product was then added and positioned such that it was in close agreement with its observed position in the X-ray crystal structure of the GLU-bound complex (PDB ID: 3V9K).²³ Note that the X-ray crystallographic structure of the enzyme-product complex was not used as the template for the PC model as the side chain of the critical active Glu314 was not fully crystallized. In addition, the thiol group of Cys348 was modeled as neutral in both RC and PC complexes. Although the enzyme is homo-dimeric, we have chosen to keep both monomers due to presence of interface residues.

Solvation and energy minimization

For the fully-bound wild-type reactant (RC^{GSA/NAD⁺}) and GLU-bound product (PC^{GLU}) complexes, missing hydrogen atoms were added using the MOE default method. After removing the solvent from each X-ray crystal structure, both enzyme-ligand complexes were then solvated with a 4 Å spherical layer of water molecules. To force the system to lie within the volume of space defined by the surrounding shell of water molecules, an ellipsoidal potential wall with a scaling constant of 2 was placed around the solvated enzyme-ligand complexes. To allow the electrostatic and van der Waals potentials to decay smoothly beyond 8–10 Å, a damping functional factor was included. The geometries of the solvated complexes were then optimized using the AMBER12:EHT force field until the root-mean-square gradient of the total energy fell below

Scheme 2. The three-stage mechanistic proposal for the conversion of glutamate- γ -semialdehyde to glutamate as catalyzed by P5CDH.¹⁸ [Colour online.]



0.21 kJ mol⁻¹ Å⁻¹. In addition, to reduce computational expense but retain sufficient flexibility, and as the present study is focused on gaining insight into the changes that may occur within the active site, only those residues and water molecules within the second environmental shell neighboring the P5CDH active site, <27 Å from C_{carb} of active site ligand, were free to move in both the minimizations and MD simulations.

Thermal relaxation

MD simulations were then performed under constrained pressure and temperature. The equations of motion were coupled with the Nosé-Poincaré thermostat,⁴¹ and the time step for numerical integration was set to 2 fs. Initially, the systems were heated from 150 to 300 K for a period of 100 ps, followed by a production run of 10 ns at 300 K and pressure of 1 atm (1 atm = 101.325 kPa). Based on active site RMSD and cluster analyses, a representative structure was chosen from each RC^{GSA/NAD⁺} and PC^{GLU} trajectory and then optimized using AMBER12:EHT. These optimized structures were then used as templates to generate a starting structure for all other wild-type and mutated reactant and product complexes considered (see below).

Summary of complexes considered

In total, 20 different enzyme and enzyme-ligand(s) complexes were examined and are summarized in the supporting information (Tables S1–S3) (see Supplementary material section). More specifically, as well as the above RC^{GSA/NAD⁺} and PC^{GLU} complexes, we also considered wild-type reactant complexes of P5CDH with

NAD⁺ and the alternate substrate 4-OH-GSA bound in the active site, or with only NAD⁺ or GSA bound. In addition, an MC (GSA- and NAD⁺-bound) containing an activated (deprotonated) Cys348 (Cys348S⁻) and neutral Glu314 (Glu314COOH) was used to examine the possible role of Glu314 in acylation. An unbound (i.e., no GLU bound) product complex (PC) was also examined. Several genetically important *in silico* mutations (S352L, S352A, and E314A) were performed on the RC^{GSA/NAD⁺} and PC^{GLU} complexes (i.e., generated using PDB ID: 3V9L or 3V9J, respectively),²³ and the structures of their fully-bound (NAD⁺ + substrate for RCs and GLU for PCs) and unbound active site structures investigated. Collectively, these models were selected as they enabled us to examine multiple aspects that may affect active site structure, including ionization states of key residues, binding of ligands, and their possible bound orientations. For these additional complexes the same simulation procedure as described in the Thermal relaxation section was applied, with the exception that a 5 ns production run was used instead. All of these calculations were subjected to several RMSD and cluster analyses, resulting in average structures. Each model representative was then used for geometric and comparison analysis to other complexes. We have successfully applied this MD protocol in the study of other enzymatic systems.^{42–43}

Results and discussion

Reactant and product Michaelis complexes

As noted in Computational methods, we first examined the flexibility of the fully bound wild-type reactant (RC^{GSA/NAD⁺}) and

Fig. 1. Plots of the RMSDs obtained during the 100 ps thermal relaxation and subsequent 10 ns production runs of wild-type P5CDH with (A) GSA + NAD⁺ ($\text{RC}^{\text{GSA/NAD}^+}$) or (B) GLU (PC^{GLU}) bound within its active site (see text). [Colour online.]

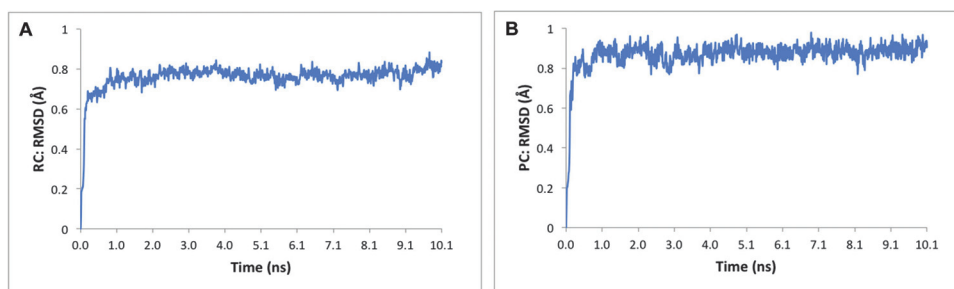
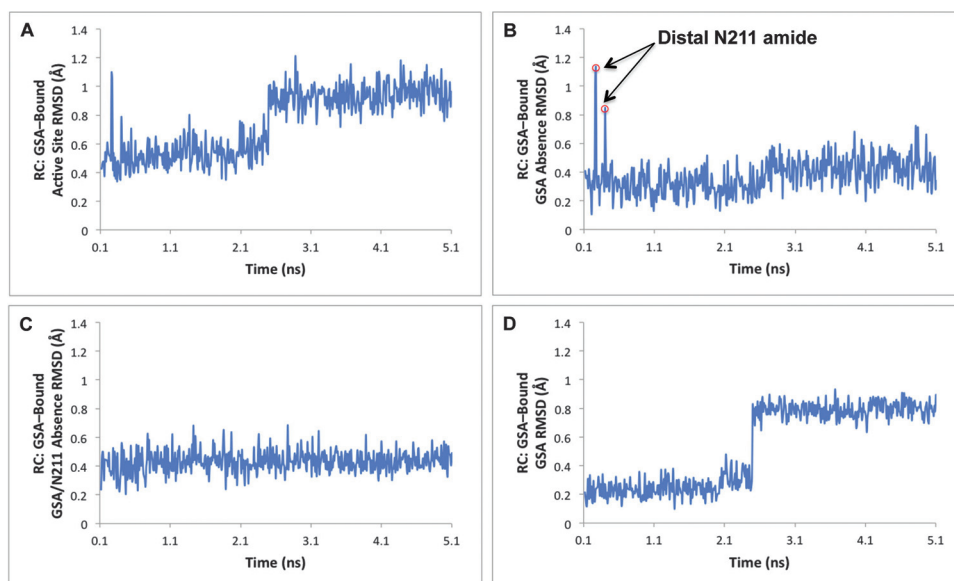


Fig. 2. Plots of the RMSDs obtained for RC^{GSA} (A) with inclusion of GSA, or excluding (B) only the GSA, or (C) both GSA and the Asn211 amide, or (D) all but the GSA substrate. [Colour online.]



product (PC^{GLU}) complex active sites. More specifically, we considered the RMSDs of key residues in and around the active site, associated water molecules, and bound-ligands during 10 ns simulations, which are plotted in Fig. 1. That is, we first examined from a broader perspective the flexibility over time of the bound active sites and surrounding environment. It should be noted that the large initial increase in RMSD occurs during the 100 ps thermal relaxation period and is simply included for completeness.

More importantly, during the 10 ns production run the RMSDs for $\text{RC}^{\text{GSA/NAD}^+}$ lie within a relatively narrow range of $0.57 \pm 0.10 \text{ \AA}$ (Fig. 1A). Similarly, the RMSDs for the GLU-bound product complex PC^{GLU} also lie within a narrow range of just $0.39 \pm 0.08 \text{ \AA}$ (Fig. 1B). It should be noted that for these RMSD calculations the residues Cys348, Glu314, Asn211, GLU, and mechanistic water near Glu314 were used. This lower variability may be due in part to the lack of the flexible NAD⁺ coenzyme in PC^{GLU} unlike $\text{RC}^{\text{GSA/NAD}^+}$.

Ligand-bound reactant complexes

To gain more detailed insights into the dynamics of the bound active sites, as noted in Computational methods, average structures were obtained of $\text{RC}^{\text{GSA/NAD}^+}$ and PC^{GLU} from the 10 ns runs and used as templates for starting structures of several different wild-type enzyme–ligand complexes (Tables S1 and S3). MD simulations were then run on these complexes for 5 ns to ensure conformational equilibrium was achieved.

For the RC complex with only GSA bound in the active site (RC^{GSA}), the calculated RMSDs included not only GSA, but also the R-group thiol, carboxyl, and amide of Cys348, Glu314, and Asn211,

respectively, and the peptide backbone between Cys348 and Lys347, and is plotted in Fig. 2A. As can be seen, after approximately 2.5 ns there is a marked shift in RMSD values from around approximately 0.5 to 0.9 Å, which remains around there until the end of the simulation. As a result, the RMSDs over the course of the simulation have a much broader range of $0.87 \pm 0.22 \text{ \AA}$ than observed for the fully bound reactant complex $\text{RC}^{\text{GSA/NAD}^+}$.

This variability was investigated via cluster analysis, grouping the RMSDs into five clusters. A representative structure of each cluster was selected and overlaid as seen in Fig. 3A. As can be seen, the largest variation appears to occur in the position of the aldehyde of the GSA substrate and the R-group carboxylate of Glu165. However, to better understand the contributions of the various components, cluster analysis of the RMSDs was also performed in which the (i) GSA, or (ii) GSA and Asn211 amide were excluded from the analysis, Figs. 2B and 2C respectively, and (iii) only the RMSDs of the GSA were considered (Fig. 2D).

When the GSA substrate is excluded from the RMSD analysis, the RMSDs are low and all fall within a very narrow range (see Fig. 2B). The spikes observed correspond to the Asn211 amide side chain undergoing very short-lived conformational shifts. Specifically, it becomes distal with respect to the substrate's carbonyl oxygen (O_{carb}), significantly increasing the $\text{O}_{\text{carb}} \cdots \text{HN}_{211}$ distance from 6.29 (average) to 8.17 Å (Table 1). Regardless, there is no hydrogen bond formed between O_{carb} and Asn211's amide, a proposed key interaction in the oxyanion hole. This may be due to the absence of bound NAD⁺ coenzyme.

Fig. 3. Overlays of representative structures obtained from cluster analysis of the RMSDs of RC^{GSA} (A) with inclusion of GSA, excluding (B) the GSA substrate, or (C) both GSA and the Asn211 amide, and (D) all but the GSA substrate. Note, some additional functional groups not used in the RMSD calculations are also shown (see text). [Colour online.]

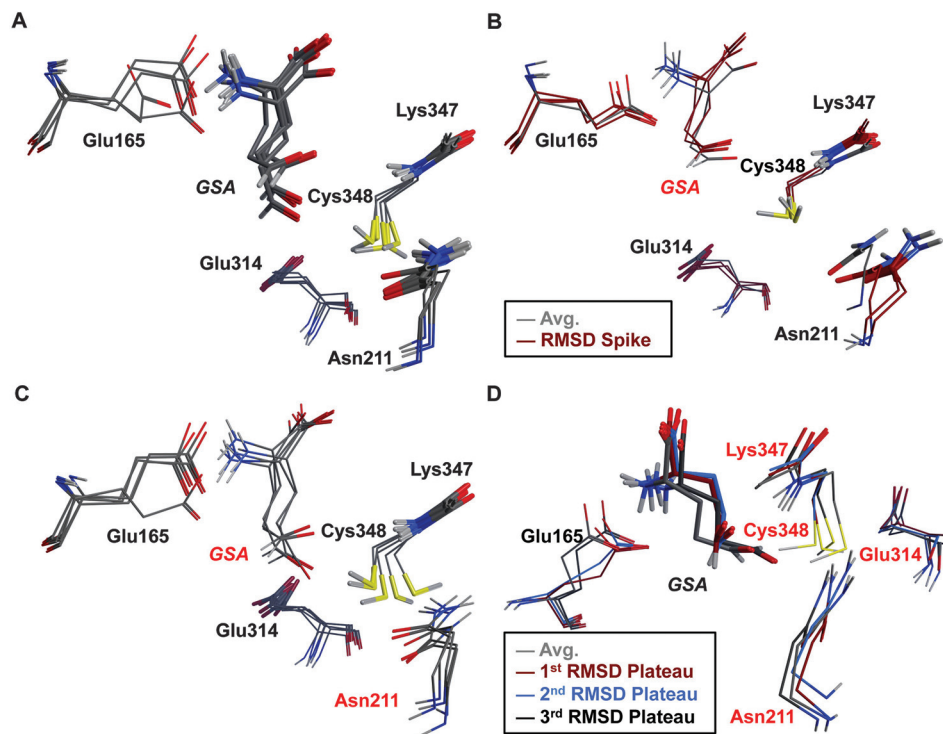


Table 1. Select average distances (Å) of RC^{GSA} corresponding to structures shown in Fig. 3.

Structure	$C_{carb} \cdots S_{C348}$	$O_{carb} \cdots HS_{C348}$	$O_{carb} \cdots HN_{C348}$	$O_{carb} \cdots HN_{N211}$
Avg. B	4.38	2.66	3.68	6.29
Spike	4.83	3.35	3.80	8.17
Avg. D	5.14	3.13	3.76	5.32
1st plateau	3.67	4.57	3.03	4.90
2nd plateau	3.84	2.01	3.20	5.30
3rd plateau	4.12	1.91	4.24	4.41

When the RMSDs are recalculated, but now excluding both GSA and Asn211, they now fall in a quite narrow range of only 0.48 ± 0.07 Å (Fig. 2C). As can be seen from the overlaid representative structures (Fig. 3C), the remaining residues maintain relatively consistent positions, with the minor exception of the thiol proton of Cys348 which rotates in and out of the active site. This is perhaps expected due to the lack of structural constraints imposed by, for instance, an oxyanion hole.

Finally, when only the RMSDs of the GSA in RC^{GSA} are considered (Figs. 2D and 3D), it appears that after 1.8–1.9 ns the initial bound conformer of GSA (with average RMSD of ~ 0.2 Å) shifts to a short lived (~ 0.5 ns) second conformation (with average RMSD of ~ 0.3 Å) before shifting to a third and longer lived conformation for the last 2.6 ns of the simulation (with an average RMSD of just over 0.8 Å). Each of these RMSD conformational plateaus has quite a small variability, with the largest range being 0.30 ± 0.05 Å, and the small differences between each of the conformers is illustrated in Fig. 3D. For each of these conformations, select average interaction distances were also calculated. Notably, the mechanistically relevant average $C_{carb} \cdots S_{C348}$ distances were quite long at, in order of occurrence of conformation in the MD simulation, 3.67, 3.84, and 4.12 Å. Similarly, the distances between GSA's O_{carb} centre and the proposed oxyanion hydrogen bond donors R-group $-NH_2$ of Asn211 and backbone $-NH-$ of C348 are also

moderately large with their shortest average lengths being 3.03 and 4.41 Å, respectively. These results also suggest that in the absence of bound NAD^+ coenzyme the GSA-bound active site may not be consistently favourably positioned for catalysis.

It is noted that in addition to the fully bound reactant complex (RC^{GSA/NAD^+}), we also performed MD simulations and cluster analysis on an RC^{NAD^+} complex (i.e., only NAD^+ bound), and RC^{GSA/NAD^+} derived structure with no GSA or NAD^+ bound (RC^{NL}). Importantly, in the fully bound RC^{GSA/NAD^+} complex the average $r(C_{carb} \cdots S_{C348}) = 4.13$ Å (see Table 2), 0.25 Å closer than in RC^{GSA} . Similarly, the suggested oxyanion hole interactions $r(O_{carb} \cdots HN_{C348}) = 3.29$ Å and $r(O_{carb} \cdots HN_{N211}) = 5.39$ Å, are 0.39 and 0.90 Å shorter, respectively. Nevertheless, these distances still seem mechanistically too long with respect to GSA's aldehyde group, suggesting that the substrate or residues may not yet be suitably positioned for reaction.

However, it was observed that in RC^{GSA/NAD^+} the R-group carboxyl of Glu447 hydrogen bonds with the ribose moiety of the NAD^+ , in agreement with experiment.²³ In contrast, in RC^{GSA} the glutamyl side chain hydrogen bonds with the R-group hydroxyl of Ser287 (Fig. S4), suggesting Glu447 has a role in NAD^+ binding as proposed by Srivastava and co-workers.²³

Ligand-bound product complexes

For the GLU-bound PC (PC^{GLU} ; Table 3), the active site calculated RMSDs included not only GLU, but also the R-group thiol, carboxyl, and amide of Cys348, Glu314, and Asn211, respectively, and the peptide backbone between Cys348 and Lys347, and are plotted in Fig. 4A. It can be seen that these overall RMSDs occur in the range of 0.56 ± 0.14 Å. However, frequent fluctuations were observed over the course of the simulation.

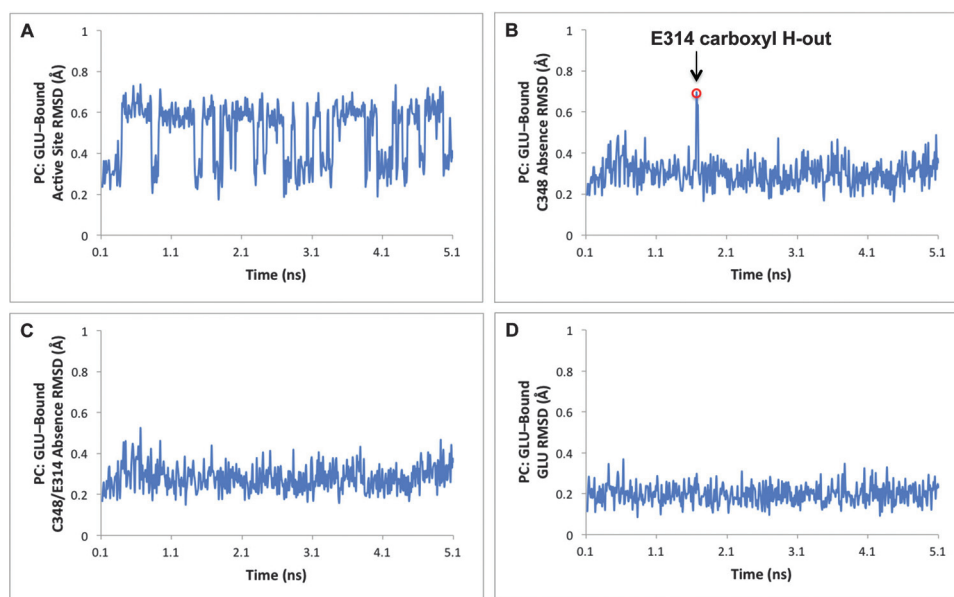
Insight into these fluctuations can be obtained by cluster analysis of the RMSDs and overlaying a representative structure from each of the five clusters (Fig. 5A). Many of the proposed mechanistic interactions (e.g., oxyanion hole) are reasonably consistent over the period of the simulations. For example, the $O_{carb} \cdots HN_{C348}$ and $O_{carb} \cdots HN_{N211}$ distances are 1.88 and 1.87 Å, respectively, indi-

Table 2. Select average distances (Å) for $\text{RC}^{\text{GSA/NAD}^+}$, $\text{actRC}^{\text{GSA/NAD}^+}$, and $\text{RC}^{\text{4GSA/NAD}^+}$.

Structure	$\text{C}_{\text{carb}} \cdots \text{S}_{\text{C348}}$	$\text{O}_{\text{carb}} \cdots \text{HS}_{\text{C348}}$	$\text{O}_{\text{carb}} \cdots \text{HN}_{\text{C348}}$	$\text{O}_{\text{carb}} \cdots \text{HN}_{\text{N211}}$	$\text{C}_{\text{pyr}} \cdots \text{S}_{\text{C348}}$	$\text{C}_{\text{pyr}} \cdots \text{H}_{\text{carb}}$
$\text{RC}^{\text{GSA/NAD}^+}$	4.13	2.81	3.29	5.39	3.54	7.20
$\text{actRC}^{\text{GSA/NAD}^+}$	3.55	N/A	2.21	4.52	3.65	6.39
$\text{RC}^{\text{4GSA/NAD}^+}$	4.17	2.04	3.75	4.58	3.81	7.83

Table 3. Select average distances (Å) for $\text{S352 LRC}^{\text{GSA/NAD}^+}$, S352 LRC , $\text{S352 LPC}^{\text{GLU}}$ and S352 LPC .

Structure	$\text{C}_{\text{carb}} \cdots \text{S}_{\text{C348}}$	$\text{O}_{\text{carb}} \cdots \text{HS}_{\text{C348}}$	$\text{O}_{\text{carb}} \cdots \text{HN}_{\text{C348}}$	$\text{O}_{\text{carb}} \cdots \text{HN}_{\text{N211}}$	$\zeta \text{C}_{\text{E449}} \cdots \alpha \text{C}_{\text{C348}}$	$\partial \text{C}_{\text{E447}} \cdots \alpha \text{C}_{\text{C348}}$
$\text{S352 LRC}^{\text{GSA/NAD}^+}$	4.49	4.74	3.89	4.86	8.03	6.76
S352 LRC	N/A	N/A	N/A	N/A	3.98	11.29
$\text{S352 LPC}^{\text{GLU}}$	5.12	5.23	1.87	1.81	4.44	7.49
S352 LPC	N/A	N/A	N/A	N/A	4.81	9.19

Fig. 4. Plots of the RMSDs obtained for PC^{GLU} (A) with inclusion of GLU, and excluding (B) the thiol of Cys348 or (C) both the thiol of Cys348 and R-group carboxyl of Glu314, or (D) all but the GLU product. [Colour online.]

cating that they are moderately strong hydrogen bonds, and vary by 0.18 and 0.29 Å, respectively. In contrast, the positioning of the Cys348 thiol, and hence its interactions, are considerably more variable. In particular, the $\text{C}_{\text{carb}} \cdots (\text{H})\text{S}_{\text{C348}}$ and $\text{O}_{\text{carb}} \cdots \text{HS}_{\text{C348}}$ distances fluctuate by as much as 1.55 and 3.19 Å, respectively. In addition, the $\angle \text{N}-\alpha\text{C}-\beta\text{C}-\text{S}$ angle of Cys348 varies between -27.9 and -153.7° . As noted in the Introduction, release of the GLU product is thought to require the Cys348 thiol group to reposition away from the catalytic site. The fluctuations in Fig. 4A illustrate that this process occurs reasonably regularly as an interconversion between the thiol being inside (~ 0.3 Å RMSD region) and outside (~ 0.6 Å RMSD region) the active site over the course of the 5 ns simulation. Lastly, the average $\partial \text{C}_{\text{E314}} \cdots (\text{H})\text{S}_{\text{C348}}$ distance in PC^{GLU} was 4.08 Å (not shown), whereas in $\text{RC}^{\text{GSA/NAD}^+}$ the average $\partial \text{C}_{\text{E314}} \cdots (\text{H})\text{S}_{\text{C348}}$ distance is 10.26 Å (not shown). Thus, the carboxyl of Glu314 may be better placed to act as the base in the deacylation stage of the mechanism.

Analogous to that detailed above for $\text{RC}^{\text{GSA/NAD}^+}$, greater insights into the role and behavior of key residues and the product was obtained by reanalyzing the above RMSDs but excluding specific selected group(s). The resulting RMSDs and overlaid representative structures obtained via cluster analysis for each complex are shown in Figs. 4 and 5. In the absence of the carboxylate of Glu314 and (or) thiol of Cys348, the RMSDs of the remaining active site residues (Figs. 4B and 4C), and corresponding representative structures (Figs. 5B and 5C), show greater consistency as illus-

trated by RMSD ranges of 0.37 ± 0.06 and 0.52 ± 0.06 Å, respectively. Finally, when only the RMSDs of the GLU product are considered, we can see from Fig. 4D that the resulting plot indicates little conformational variation (0.28 ± 0.05 Å) over the course of the simulation. Collectively, these additional analyses suggest that the source of the large fluctuations in Fig. 4A are due to the high positional variability of the Cys348 thiol in PC^{GLU} .

In unbound PC (PC^{NL}) the calculated RMSDs reached convergence within the first 0.50 ns (Fig. S5). Notably, the oxyanion hole collapsed, resulting in rapid repositioning of the Asn211 amide and Cys348 $-\text{NH}-$ backbone away from the active site with $\angle \Delta (\text{N}-\alpha\text{C}-\beta\text{C}-\delta\text{C}) = 94.0^\circ$ and $\angle \Delta (\text{N}-\alpha\text{C}-\beta\text{C}-\text{S}) = 103.7^\circ$, respectively (Fig. S6). These conformational changes provide more space within the active site for entrance and binding of GSA and NAD^+ .

Activated and hydroxylated-Michaelis complexes

As stated in the Introduction it has been suggested that Glu314 may act as a base and abstract the Cys348 thiol proton, thereby activating P5CDH for catalysis.^{28,32} Using a fully bound activated enzyme complex, i.e., NAD^+ and GSA ($\text{actRC}^{\text{GSA/NAD}^+}$) or 4-hydroxylated GSA (4-OH-GSA; $\text{actRC}^{\text{4GSA/NAD}^+}$) bound with an anionic Cys348 (Cys348S^-) and neutral Glu314 (Glu314COOH), we examined the structural and binding consequences of such an activation. The resulting plots of RMSD versus time are shown in Fig. 6.

Fig. 5. Overlays of representative structures obtained from cluster analysis of the RMSDs of PC^{GLU} (A) with inclusion of GLU, excluding (B) the thiol of Cys348, or (C) both the thiol of Cys348 and R-group carboxyl of Glu314, and (D) all but the GLU product. Note that some additional functional groups not used in the RMSD calculations are also shown (see text). [Colour online.]

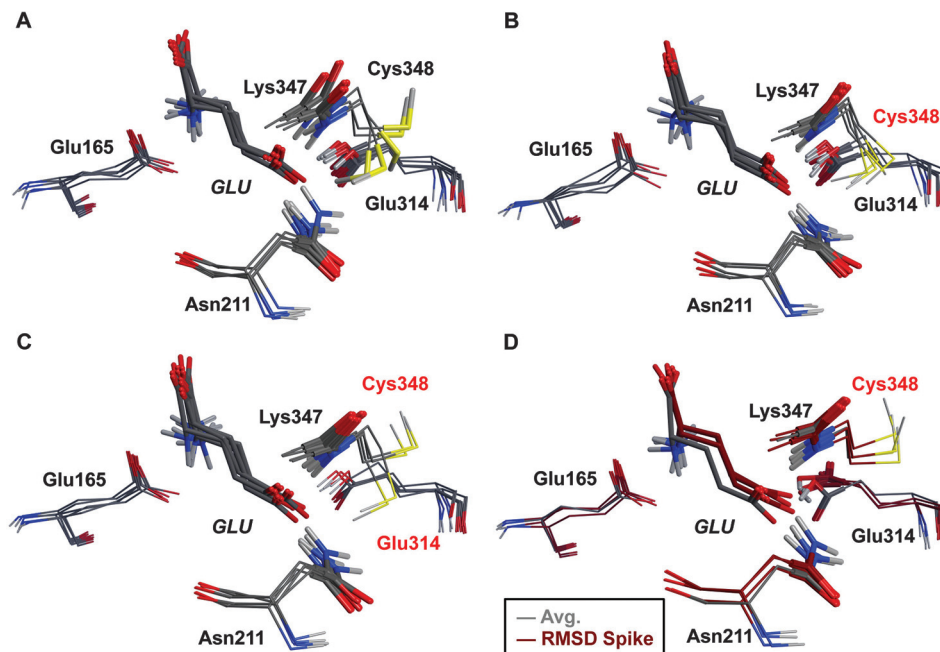
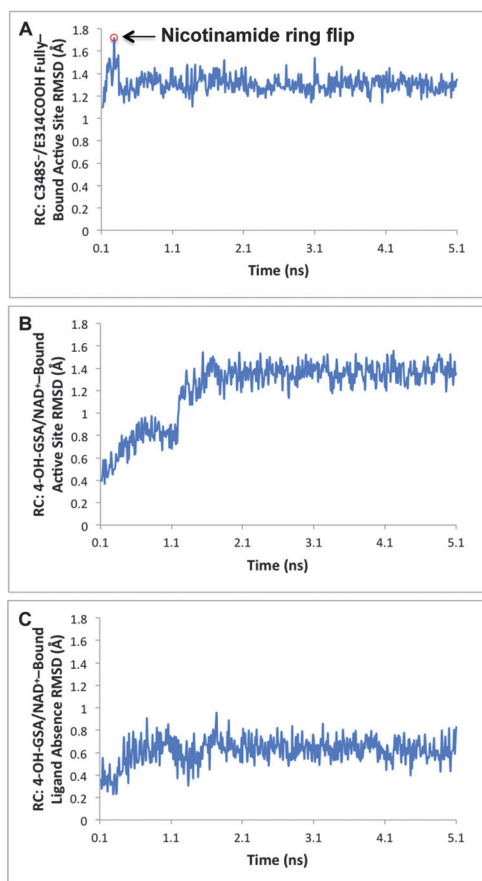


Fig. 6. Plots of the RMSDs obtained for the fully bound $actRC$ complexes containing (A) GSA, (B) 4-OH-GSA, and (C) the active enzyme with only NAD^+ bound ($actRC^{NAD^+}$). [Colour online.]



In the plot of RMSDs for $actRC^{GSA/NAD^+}$, Fig. 6A, a spike in RMSDs is observed near initiation of the simulation. This is due to repositioning of the NAD^+ coenzyme. However, once repositioned, the RMSDs are quite consistent, as also evidenced by the consistent overlay of the five representative structures obtained from cluster analysis (Fig. 7A). A comparison of the average structures of $actRC^{GSA/NAD^+}$ with the fully bound 'unactivated' RC^{GSA/NAD^+} complex is shown in Fig. 8A. Importantly, it can be seen that the mechanistically important $C_{carb} \cdots (H)S_{C348}$ distance in the activated form is considerably shorter by 0.58 Å at 3.55 Å, than in RC^{GSA/NAD^+} . Furthermore, the oxyanion hole-relevant distance $O_{carb} \cdots HN_{N211}$ is also markedly shorter at 2.21 Å and can now in fact be thought of as at least a weak hydrogen bond. The distance between the hydride acceptor site in the NAD^+ (C_{pyr}) and substrate hydride to be abstracted (H_{carb}) is 0.81 Å shorter at 6.39 Å in $actRC^{GSA/NAD^+}$. Presumably, this shorter distance would help facilitate the required hydride transfer to NAD^+ . Collectively, these results suggest that the presence of an anionic Cys348 thiolate aids in positioning of the substrate, coenzyme, and key active site residues for reaction.

A previous crystallographic study on a related member of the aldehyde dehydrogenase family,³² suggested that there may be two active site conformations; in one the cysteinyl sulfur and C4 of the nicotinamide ring are covalently cross-linked, while in the other they are not and lie 2.60 Å apart. In the present study the average $r(C_{pyr} \cdots S_{C348})$ distance is quite large at 3.65 Å, and the nicotinamide ring is still planar (Table 2). Furthermore, the anionic charge on the Cys348 thiolate is stabilized by hydrogen bonds with the R-group amide of Asn211, average $r(S_{C348} \cdots HN_{N211}) = 2.19$ Å, and the amide moiety of the nicotinamide ring with an average $r(S_{C348} \cdots HN_{pyr})$ of 2.09 Å (see also Fig. 8A). It is noted that the latter amide moiety is flipped with respect to its position in the "unactivated" RC^{GSA/NAD^+} complex. This conformation of the "activated" RC^{GSA/NAD^+} complex, $actRC^{GSA/NAD^+}$, appears to be dominant at equilibrium, as might be expected if Cys348S⁻ is to act as the nucleophile.

P5CDH is also able to catalyze the oxidation the 4-hydroxylated derivative of GSA, 4-OH-GSA.²⁷ Hence, for completeness, we also examined the structural consequences of this substrate hydroxylation on the fully bound (neutral Cys348 thiol) enzyme, RC^{4GSA/NAD^+} .

Fig. 7. Overlays of representative structures obtained from cluster analysis of the RMSDs of ${}^{\text{act}}\text{RC}^{\text{NAD}^+}$ in which GSA is (A) included or (B) not included in RMSD calculation, and in which 4-OH-GSA is (C) included or (D) not included in RMSD calculation. Note that some additional functional groups not used in the RMSD calculations are also shown (see text). [Colour online.]

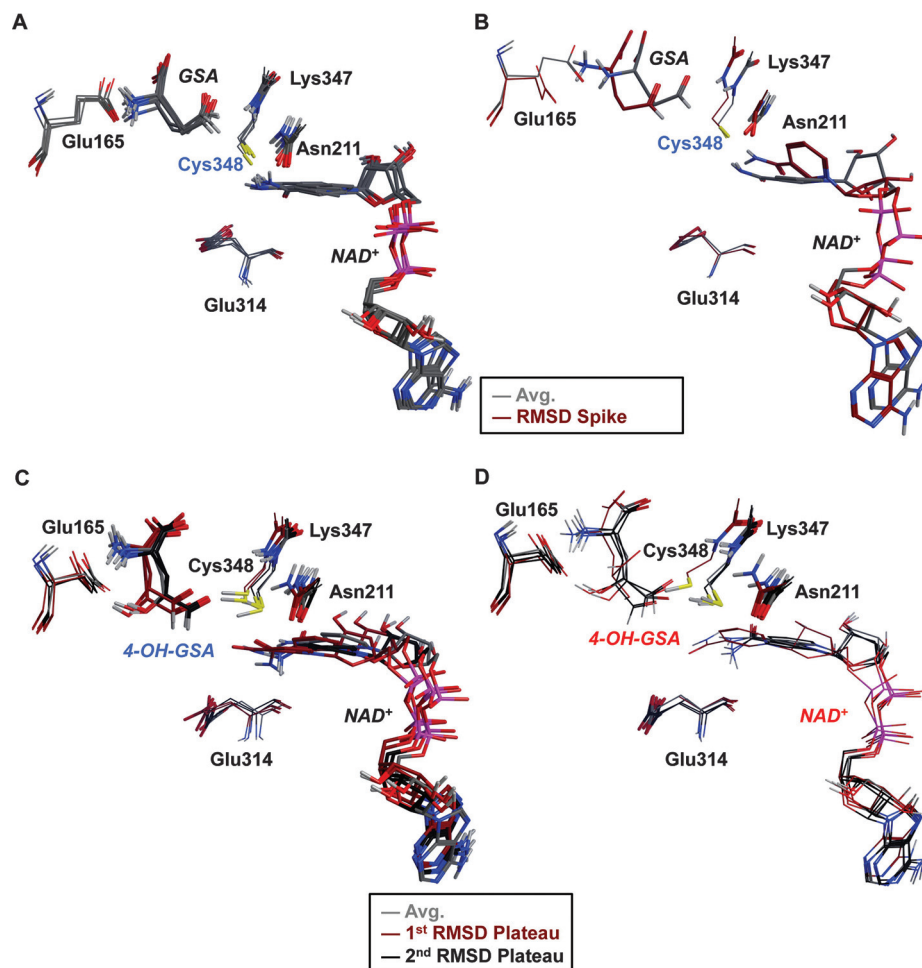
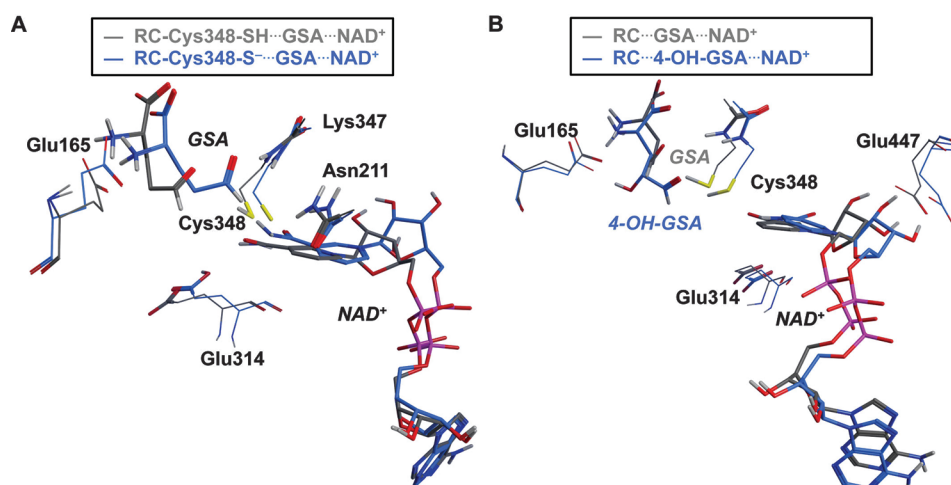


Fig. 8. Overlays of average structures of the (A) fully bound reactant complex $\text{RC}^{\text{GSA}/\text{NAD}^+}$ in both its unactivated and active states and (B) unactivated fully bound reactant complexes of GSA or 4-OH-GSA bound. Note that some additional functional groups not used in the RMSD calculations are also shown (see text). [Colour online.]

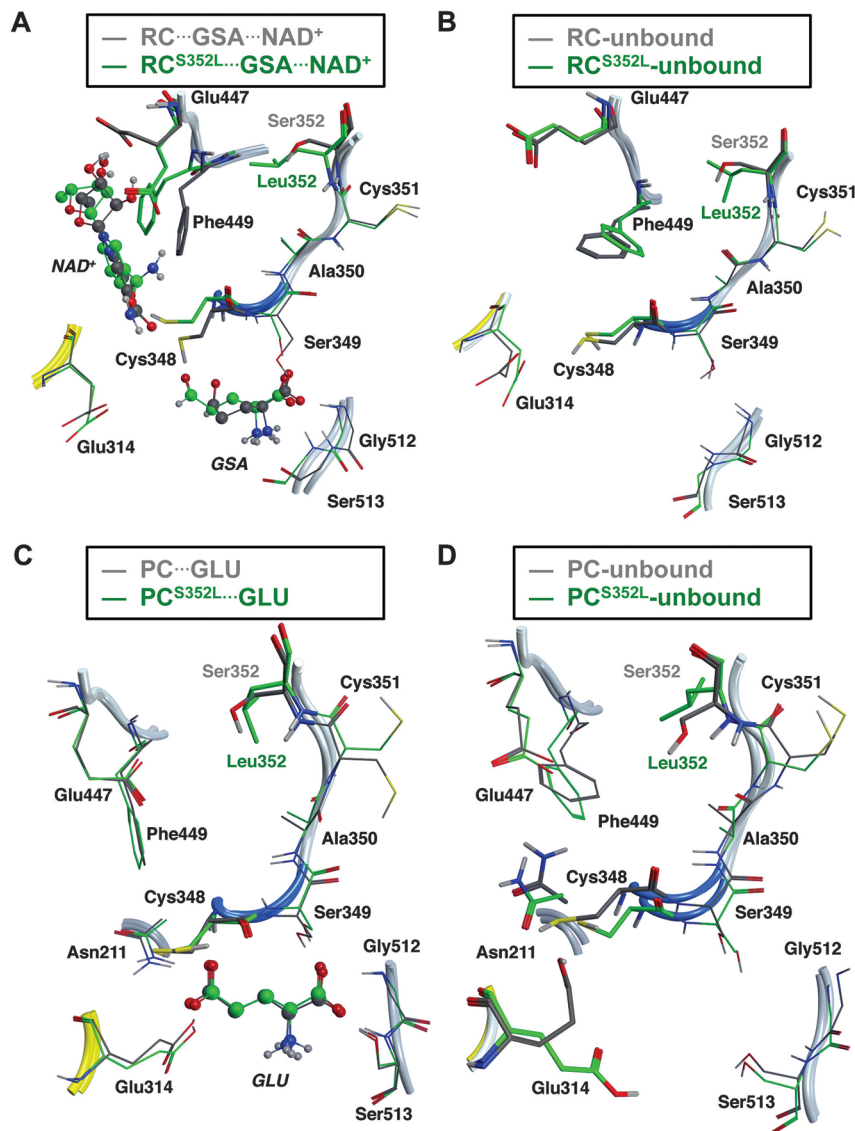


The plot of the RMSDs for this complex over the course of the simulation are shown in Fig. 6B, while overlaid representative structures are shown in Figs. 7C and 7D. As can be seen, all values lie within a very narrow range of $0.48 \pm 0.09 \text{ \AA}$ range. To further

illustrate any structural differences with the initial $\text{RC}^{\text{GSA}/\text{NAD}^+}$ complexes, we have overlaid their average structures in Fig. 8B.

The γ -hydroxyl group of 4-OH-GSA maintains a consistent strong hydrogen bond interaction with the R-group carboxyl of

Fig. 9. Overlays of average structures of the wild-type and S352L mutated (A) fully bound ($\text{RC}^{\text{GSA/NAD}^+}$ and $\text{S}^{352\text{L}}\text{RC}^{\text{GSA/NAD}^+}$) and (B) unbound (RC and $\text{S}^{352\text{L}}\text{RC}$) reactant complexes, and (C) fully bound (PC^{GLU} and $\text{S}^{352\text{L}}\text{PC}^{\text{GLU}}$) and (D) unbound (PC and $\text{S}^{352\text{L}}\text{PC}$) product complexes. [Colour online.]



Glu165, average $r(\text{HO}_{4\text{-OH-GSA}} \cdots \text{OOC}_{\text{E165}}) = 1.63 \text{ \AA}$. In addition, in $\text{RC}^{\text{4GSA/NAD}^+}$ the average $r(\text{C}_{\text{carb}} \cdots \text{S}_{\text{C348}})$ distance of 4.17 \AA is just 0.04 \AA longer than in $\text{RC}^{\text{GSA/NAD}^+}$ (Table 2). Consequently, the 4-OH-GSA and GSA substrates are similarly positioned within the active site. In contrast, the coenzyme's nicotinamide ring appears to shift away from the active site with its amide moiety now flipped (see above; Figs. 7C, 7D, and S7). Importantly, due to the coenzyme's positioning, the $\text{C}_{\text{pyr}} \cdots (\text{H})\text{S}_{\text{C348}}$ and $\text{C}_{\text{pyr}} \cdots \text{H}_{\text{carb}}$ distances in $\text{RC}^{\text{4GSA/NAD}^+}$ are longer compared to $\text{RC}^{\text{GSA/NAD}^+}$ by 0.27 and 0.63 \AA with average distances of 3.81 and 7.83 \AA , respectively (Fig. 7C and Table 2). These longer interactions also suggest that the hydride transfer from GSA/4-OH-GSA to NAD^+ may be less facile when Cys348 has a neutral thiol.

Effects of selected mutations

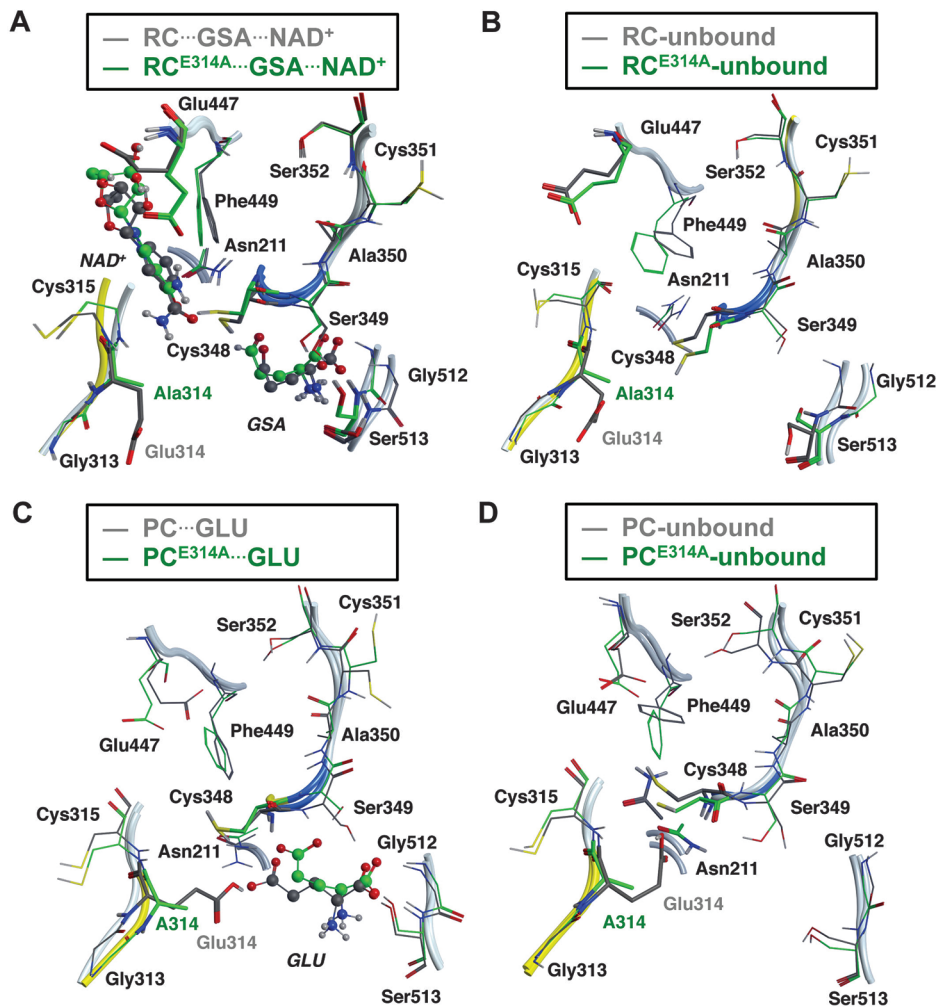
It has been experimentally shown that several physiological disorders, e.g., type II hyperprolinemia, may be associated with certain P5CDH genetic mutations. Hence, the effects of several possible mutations on the structure of the active site and substrate binding were examined.

S352L

The mutation of Ser352 to Leu has been suggested to reduce the enzymatic activity of P5CDH through, at least in part, changes in the positioning of several key residues or their interactions.^{1,38} It has been experimentally shown to render the enzyme inactive and unable to bind NAD^+ .¹ We constructed several possible S352L mutant reactant-derived ($\text{S}^{352\text{L}}\text{RC}^{\text{GSA/NAD}^+}$, $\text{S}^{352\text{L}}\text{RC}$) and product-derived ($\text{S}^{352\text{L}}\text{PC}^{\text{GLU}}$, $\text{S}^{352\text{L}}\text{PC}$) complexes in both fully-bound and unbound states. The resulting average structure obtained for each complex is overlaid with its corresponding wild-type enzyme complex in Fig. 9.

For $\text{S}^{352\text{L}}\text{RC}^{\text{GSA/NAD}^+}$ (Fig. 9A) it can be seen that upon mutation, large positional changes are observed for Phe449 and Glu447. Relative to the corresponding fully bound wild-type enzyme complex $\text{RC}^{\text{GSA/NAD}^+}$ the average $r(\text{C}_{\text{E449}} \cdots \alpha\text{C}_{\text{C348}})$ and $r(\beta\text{C}_{\text{E447}} \cdots \alpha\text{C}_{\text{C348}})$ have changed by 4.11 and 4.35 \AA , respectively to 8.03 and 6.76 \AA (Table 3). As a result, the hydrophobic R-group of Leu352 clashes sterically with the phenyl ring of Phe449, disrupting the hydrogen bond between the R-group carboxylate of Glu447 and 3'-OH of NAD^+ 's ribose. The latter observation is in agreement with exper-

Fig. 10. Overlays of average structures of the wild-type and E314A mutated (A) fully bound ($\text{RC}^{\text{GSA/NAD}^+}$ and $\text{E314A}\text{RC}^{\text{GSA/NAD}^+}$) and (B) unbound (RC and $\text{E314A}\text{RC}$) reactant complexes, and (C) fully bound (PC^{GLU} and $\text{E314A}\text{RC}^{\text{GLU}}$) and (D) unbound (PC and $\text{E314A}\text{PC}$) product complexes. [Colour online.]



iment,¹ where the S352L mutation was concluded to cause Glu447 to no longer bind NAD^+ . In the present simulation, its loss causes the NAD^+ moiety to shift markedly away from the GSA and active site. It is noted that one limitation of the present in silico mutagenesis studies is that the NAD^+ moiety is unable to completely leave the binding site. Experimentally¹ the Cys348 thiol was suggested to face the wrong way for reaction with the substrate. However, in the present model the significant shift in the position of the NAD^+ results in the Cys348 thiol rotating away from the GSA substrate with a marked increase in the distance between the substrate's aldehyde carbon (C_{carb}) and Cys348 sulfur of 0.22 Å (Table 3). It is also noted that experimentally¹ the S352L mutation was also suggested to disrupt the Ser349...substrate interaction. In the present model a shift in the position of the side chain of Ser349 away from the GSA substrate is observed (Fig. 9A). In contrast, comparison of the unbound wild-type and S352L mutant enzyme (RC , $\text{S352L}\text{RC}$), Fig. 9B, indicates that the mutations greatest effect is on the positioning of the aromatic phenyl ring of Phe449.

For the product-derived complexes, $\text{S352L}\text{PC}^{\text{GLU}}$ and $\text{S352L}\text{PC}$, the S352L mutation appears to have little effect on the active site of P5CDH and binding of GLU (Figs. 9C and 9D). In the last stage of the overall catalytic mechanism of P5CDH (deacylation), the NADH coenzyme formed is thought to be absent to enable a water to become available for the required hydrolysis.

We also performed in silico mutagenesis studies in which Ser352 was replaced by alanine. That is, the R-group hydroxyl of Ser352 was simply replaced by a hydrogen, thus removing the effects of increased steric bulk introduced through the S352L mutation. Importantly, for all of the corresponding reactant- and product-derived complexes considered, the absence of the seryl side chain hydroxyl $-\text{OH}$ did not cause any major conformational changes in the active sites (Fig. S13 and Table S6). This further supports the suggestion that it is the bulky hydrophobic side chain of the leucyl in the S352L that induces the conformational changes in the active site.

E314A

In earlier experimental³² studies on 10-formyltetrahydrofolate dehydrogenase, mutation of Glu673 (equivalent of Glu314 in P5CDH) to an alanine, resulted in inactivation of the enzyme.³² It was thus suggested that the glutamyl may be involved in substrate acylation. Consequently, to examine the role of Glu314 in acylation, we constructed several E314A mutant reactant- ($\text{S352L}\text{RC}^{\text{GSA/NAD}^+}$, $\text{S352L}\text{RC}$) and product-derived ($\text{S352L}\text{PC}^{\text{GLU}}$, $\text{S352L}\text{PC}$) complexes in both their fully bound and unbound states. The resulting average structure obtained for each complex is overlaid with its corresponding wild-type enzyme complex in Fig. 10.

Similar to that observed in the S352L mutants, the E314A mutation disrupts the hydrogen bond between the side chain carboxylate of Glu447 and 3'-OH moiety of NAD⁺'s ribose. Again, the lack of this interaction in the fully bound ^{E314A}RC^{GSA/NAD⁺} complex, as in the corresponding S352L mutant ^{S352L}RC^{GSA/NAD⁺}, results in a repositioning of the NAD⁺ moiety. In addition, the Cys348 thiol now hydrogen bonds to the carbonyl oxygen (O_{carb}) of the coenzyme's nicotinamide ring, again consistent with that also observed in the case of the S352L mutation. Although, at least with regard to the position of NAD⁺ in the active site, the outcome of these mutations is the same, they do exhibit several differences. In particular, the average $r(\zeta_{C_{F449}} \cdots \alpha C_{C348})$ distance is 3.77 Å (not shown), meaning that the Phe449 residue has not shifted significantly, and thus is not the cause of the loss of the Glu447...NAD⁺ interaction in the case of a E314A mutation. Instead there is a significant change in the backbone between Ala314 and Cys315. This likely results in the observed shift of the NAD⁺ away from the active site (Fig. 10A). Upon mutating Glu314 to alanine there is also an observed shift in the position and side chain of Glu447 for all four mutant complexes considered, with the largest impacts being seen in the fully bound reactant (^{E314A}RC^{GSA/NAD⁺}) or product (^{E314A}PC^{GLU}) complexes as can be seen in Fig. 10.

Conclusions

We have performed a MD simulations-based investigation of the active site of the aldehyde dehydrogenase Δ^1 -pyrroline-5-carboxylate dehydrogenase (P5CDH), and the binding of its substrates L-glutamate- γ -semialdehyde (GSA) and 4-erythro-hydroxy-L-glutamate- γ -semialdehyde (4-OH-GSA) and their respective L-glutamyl (GLU) type products, and coenzyme NAD⁺. In addition, we have examined the effects of activation of the Cys348 thiol, and several known physiologically important genetic mutations of P5CDH (S352L, S352A, and E314A) on the active site residues and substrate binding.

The present results suggest that in the case of a wild-type reactant enzyme complex with only GSA substrate bound (RC^{GSA}), and with a neutral active site Cys348 thiol, the substrate binds via its α -NH₃⁺ with the side chain carboxyl of Glu165, but is not suitably positioned with respect to the putative oxyanion hole. When NAD⁺ is also bound (i.e., the fully bound Michaelis complex RC^{GSA/NAD⁺}) the aldehyde carbonyl O_{carb} of GSA is positioned closer to the oxyanion hole, though still not within hydrogen bonding distance. However, when the thiol of the mechanistic nucleophile Cys348 is deprotonated (with Glu314 modeled as the base) GSA's O_{carb} centre forms a hydrogen bond with the oxyanion hole's -NH- backbone of Cys348, with an average $r(O_{carb} \cdots HN_{Cys348})$ of 2.21 Å. That is, activation of Cys348 facilitates positioning of the substrate for reaction. The Cys348 thiolate is stabilized in part by hydrogen bonds with the side chain amide of Asn211 and NAD⁺, as indicated by average $r(S_{C348} \cdots HN_{N211})$ and $r(S_{C348} \cdots HN_{pyr})$ distances of 2.19 and 2.09 Å, respectively. Our MD studies also suggest that upon loss of the product GLU, the oxyanion hole collapses shifting the Asn211 amide and Cys348 -NH- backbone away from the catalytic site. This may assist the enzyme in binding GSA and NAD⁺ for the next round of the catalytic cycle.

The S352L mutation introduces a bulky hydrophobic side chain into the active site, which sterically clashes with the phenyl of Phe449. In addition, the hydrogen bond between the side chain carboxyl of Glu447 and the NAD⁺ ribose 3'-OH group is disrupted. Similarly in the E314A mutation, the hydrogen bond between the Glu447 side chain carboxyl and 3'-OH moiety of nicotinamide ribose is broken. In the fully bound active sites of both mutants, the NAD⁺ moiety is shifted outwards from the active site. This suggests that this hydrogen bond interaction is important for the correct positioning of the NAD coenzyme. Both mutations also include a shift in the position of the thiol of Cys348 away from the substrate's aldehyde group. Collectively these structural changes

may hinder the catalytic activity of P5CDH. Indeed, in the S352A mutant, where the side chain of serinyl has been replaced by a hydrogen, such large conformational changes in the bound active sites are not observed. Furthermore, MD simulations on the four product complex models, all of which occur after the NADH formed during acylation is thought to have been released from the active site, showed comparable conformations. That is, in the reactant and product complexes, the S352L and E314A mutations have greatest effect on the initial substrate and coenzyme binding and positioning within the active site of P5CDH.

Supplementary material

Supplementary material is available with the article through the journal Web site at <http://nrcresearchpress.com/doi/suppl/10.1139/cjc-2016-0286>. Selected P5CDH active site overlays and RMSDs with respect to time used in this current work are provided in Figs. S1–S13 for select 5.1 ns MD simulations, summaries of the various models considered (Tables S1–S3), and summaries of select structural parameters of the complexes examined (Tables S4–S6).

Acknowledgements

We thank the Natural Sciences and Engineering Research Council of Canada (NSERC) for funding, Compute Canada, and Sharcnet for additional computational resources, and BFI thanks the Ontario Graduate Scholarship (OGS) program for financial support.

References

- (1) Nakamura, M.; Bhatnagar, A.; Sadoshima, J. *Circ. Res.* **2012**, *111*, 604. doi:10.1161/CIRCRESAHA.111.247924.
- (2) Kujundzic, R. N.; Zarkovic, N.; Troselj, K. G. *Crit. Rev. Eukaryotic Gene Expression* **2014**, *24*, 287. doi:10.1615/CritRevEukaryotGeneExpr.2014011828.
- (3) Ussher, J. R.; Jaswal, J. S.; Lopaschuk, G. D. *Circ. Res.* **2012**, *111*, 628. doi:10.1161/CIRCRESAHA.111.246371.
- (4) Srivastava, S. K.; Ramana, K. V.; Bhatnagar, A. *Endocr. Rev.* **2005**, *26*, 380. doi:10.1210/er.2004-0028.
- (5) Tipparaju, S. M.; Saxena, N.; Liu, S.-Q.; Kumar, R.; Bhatnagar, A. *Am. J. Physiol.: Cell Physiol.* **2005**, *288*, C366. doi:10.1152/ajpcell.00354.2004.
- (6) Liu, M.; Sanyal, S.; Gao, G.; Gurung, I. S.; Zhu, X.; Gaconnet, G.; Kerchner, L. J.; Shang, L. L.; Huang, C. L.-H.; Grace, A.; London, B.; Dudley, S. C. *Circ. Res.* **2009**, *105*, 737. doi:10.1161/CIRCRESAHA.109.197277.
- (7) Maejima, Y.; Kuroda, J.; Matsushima, S.; Ago, T.; Sadoshima, J. *J. Mol. Cell Cardiol.* **2011**, *50*, 408. doi:10.1016/j.yjmcc.2010.12.018.
- (8) Ago, T.; Kuroda, J.; Pain, J.; Fu, C.; Li, H.; Sadoshima, J. *Circ. Res.* **2010**, *106*, 1253. doi:10.1161/CIRCRESAHA.109.213116.
- (9) Hsu, C.-P.; Hariharan, N.; Alcendor, R. R.; Oka, S.; Sadoshima, J. *Autophagy* **2009**, *5*, 1229. doi:10.4161/auto.5.8.10275.
- (10) Erickson, J. R.; Joiner, M.-L. A.; Guan, X.; Kutschke, W.; Yang, J.; Oddis, C. V.; Bartlett, R. K.; Lowe, J. S.; O'Donnell, S. E.; Aykin-Burns, N. et al. *Cell* **2008**, *133*, 462. doi:10.1016/j.cell.2008.02.048.
- (11) Wang, Y.; Dawson, V. L.; Dawson, T. M. *Exp. Neurol.* **2009**, *218*, 193. doi:10.1016/j.expneurol.2009.03.020.
- (12) Stein, L. R.; Imai, S. *Trends Endocrinol. Metab.* **2012**, *23*, 420. doi:10.1016/j.tem.2012.06.005.
- (13) Dölle, C.; Rack, J. G. M.; Ziegler, M. *FEBS J.* **2013**, *280*, 3530. doi:10.1111/febs.12304.
- (14) Pollak, N.; Dölle, C.; Ziegler, M. *Biochem. J.* **2007**, *402*, 205. doi:10.1042/BJ20061638.
- (15) Ion, B. F.; Bushnell, E. A. C.; De Luna, P.; Gauld, J. W. *Int. J. Mol. Sci.* **2012**, *13*, 12994. doi:10.3390/ijms131012994.
- (16) Deuschle, K.; Funck, D.; Hellmann, H.; Däschner, K.; Binder, S.; Frommer, W. B. *Plant J.* **2001**, *27*, 345. doi:10.1046/j.1365-3113.2001.01101.x.
- (17) Deuschle, K.; Funck, D.; Forlani, G.; Stransky, H.; Biehl, A.; Leister, D.; van der Graaff, E.; Kunze, R.; Frommer, W. B. *Plant Cell* **2004**, *16*, 3413. doi:10.1105/tpc.104.023622.
- (18) Inagaki, E.; Ohshima, N.; Takahashi, H.; Kuroishi, C.; Yokoyama, S.; Tahirov, T. H. *J. Mol. Biol.* **2006**, *362*, 490. doi:10.1016/j.jmb.2006.07.048.
- (19) Slusarczyk, H.; Felber, S.; Kula, M.-R.; Pohl, M. *Eur. J. Biochem.* **2000**, *267*, 1280. doi:10.1046/j.1432-1327.2000.01123.x.
- (20) Di Pietro, E.; Sirois, J.; Tremblay, M. L.; MacKenzie, R. E. *Mol. Cell. Biol.* **2002**, *22*, 4158. doi:10.1128/MCB.22.12.4158-4166.2002.
- (21) Pemberton, T. A.; Tanner, J. J. *Arch. Biochem. Biophys.* **2013**, *538*, 34. doi:10.1016/j.abb.2013.07.024.
- (22) Van Schaftingen, E.; Rzem, R.; Marbaix, A.; Collard, F.; Veiga-da-Cunha, M.; Linster, C. L. *J. Inherited Metab. Dis.* **2013**, *36*, 427. doi:10.1007/s10545-012-9571-1.
- (23) Srivastava, D.; Singh, R. K.; Moxley, M. A.; Henzl, M. T.; Becker, D. F.; Tanner, J. J. *J. Mol. Biol.* **2012**, *420*, 176. doi:10.1016/j.jmb.2012.04.010.

- (24) Walker, V.; Mills, G. A.; Peters, S. A.; Merton, W. L. *Arch. Dis. Child.* **2000**, *82*, 236. doi:10.1136/adc.82.3.236.
- (25) Inagaki, E.; Ohshima, N.; Sakamoto, K.; Babayeva, N. D.; Kato, H.; Yokoyama, S.; Tahirov, T. H. *Acta Crystallogr. Sect. F: Struct. Biol. Cryst. Commun.* **2007**, *63*, 462. doi:10.1107/S1744309107021422.
- (26) Clelland, C. L.; Read, L. L.; Baraldi, A. N.; Bart, C. P.; Pappas, C. A.; Panek, L. J.; Nadrich, R. H.; Clelland, J. D. *Schizophr. Res.* **2011**, *131*, 139. doi:10.1016/j.schres.2011.05.006.
- (27) Valle, D.; Goodman, S. I.; Harris, S. C.; Phang, J. M. J. *Clin. Invest.* **1979**, *64*, 1365. doi:10.1172/JCI109593.
- (28) Wang, X.; Weiner, H. *Biochemistry* **1995**, *34*, 237. doi:10.1021/bi00001a028.
- (29) Farres, J.; Wang, T. T. Y.; Cunningham, S. J.; Weiner, H. *Biochemistry* **1995**, *34*, 2592. doi:10.1021/bi00008a025.
- (30) Liu, Z.-J.; Sun, Y.-J.; Rose, J.; Chung, Y.-J.; Hsiao, C.-D.; Chang, W.-R.; Kuo, I.; Perozich, J.; Lindahl, R.; Hempel, J.; Wang, B.-C. *Nat. Struct. Biol.* **1997**, *4*, 317. doi:10.1038/nsb0497-317.
- (31) Marchitti, S. A.; Brocker, C.; Stagos, D.; Vasiliou, V. *Expert Opin. Drug Metab. Toxicol.* **2008**, *4*, 697. doi:10.1517/17425255.4.6.697.
- (32) Tsybovsky, Y.; Donato, H.; Krupenko, N. I.; Davies, C.; Krupenko, S. A. *Biochemistry* **2007**, *46*, 2917.
- (33) Hammen, P. K.; Allali-Hassani, A.; Hallenga, K.; Hurley, T. D.; Weiner, H. *Biochemistry* **2002**, *41*, 7156. doi:10.1021/bi012197t.
- (34) Perez-Miller, S. J.; Hurley, T. D. *Biochemistry* **2003**, *42*, 7100. doi:10.1021/bi034182w.
- (35) Ion, B. F.; Kazim, E.; Gauld, J. W. *Molecules* **2014**, *19*, 15735. doi:10.3390/molecules191015735.
- (36) French, J. B.; Cen, Y.; Sauve, A. A.; Ealick, S. E. *Biochemistry* **2010**, *49*, 8803. doi:10.1021/bi1012436.
- (37) Kincaid, V. A.; Sullivan, E. D.; Klein, R. D.; Noel, J. W.; Rowlett, R. S.; Snider, M. J. *Biochemistry* **2012**, *51*, 545. doi:10.1021/bi201347n.
- (38) Hempel, J.; Kraut, A.; Wymore, T. *Chem.-Biol. Interact.* **2009**, *178*, 75. doi:10.1016/j.cbi.2008.10.009.
- (39) *Molecular Operating Environment (MOE)*, 2013.08; Chemical Computing Group Inc.: Montreal, QC, 2015.
- (40) Phillips, J. C.; Braun, R.; Wang, W.; Gumbart, J.; Tajkhorshid, E.; Villa, E.; Chipot, C.; Skeel, R. D.; Kalé, L.; Schulten, K. *J. Comput. Chem.* **2005**, *26*, 1781. doi:10.1002/jcc.20289.
- (41) Bond, S. D.; Leimkuhler, B. J.; Laird, B. B. *J. Comput. Phys.* **1999**, *151*, 114. doi:10.1006/jcph.1998.6171.
- (42) Bushnell, E. A. C.; Huang, W.; Llano, J.; Gauld, J. W. *J. Phys. Chem. B* **2012**, *116*, 5205. doi:10.1021/jp302556e.
- (43) De, Luna, P.; Bushnell, E. A. C.; Gauld, J. W. *J. Phys. Chem. B* **2013**, *117*, 14635. doi:10.1021/jp408486n.